International Journal of Pharmaceutics 544 (2018) 21–30

Contents lists available at ScienceDirect

International Journal of Pharmaceutics

journal homepage: www.elsevier.com/locate/ijpharm

Pharmaceutical 3D printing: Design and qualification of a single step print and fill capsule

Derrick M. Smith[a,*], Yash Kapoor[a], Gerard R. Klinzing[a], Adam T. Procopio[b]

[a] Oral Formulation Sciences and Technology, Merck & Co., Inc., 770 Sumneytown Pike, West Point, PA 19486, USA
[b] Device Development, Merck & Co., Inc., 126 E. Lincoln Ave., Rahway, NJ 07065, USA

ARTICLE INFO

Keywords:
Three dimensional printing
Fused deposition modeling
Hot melt extrusion
Burst release
Delayed release
Capsule
Additive manufacturing

ABSTRACT

Fused deposition modeling (FDM) 3D printing (3DP) has a potential to change how we envision manufacturing in the pharmaceutical industry. A more common utilization for FDM 3DP is to build upon existing hot melt extrusion (HME) technology where the drug is dispersed in the polymer matrix. However, reliable manufacturing of drug-containing filaments remains a challenge along with the limitation of active ingredients which can sustain the processing risks involved in the HME process. To circumvent this obstacle, a single step FDM 3DP process was developed to manufacture thin-walled drug-free capsules which can be filled with dry or liquid drug product formulations. Drug release from these systems is governed by the combined dissolution of the FDM capsule 'shell' and the dosage form encapsulated in these shells. To prepare the shells, the 3D printer files (extension '.gcode') were modified by creating discrete zones, so-called 'zoning process', with individual print parameters. Capsules printed without the zoning process resulted in macroscopic print defects and holes. X-ray computed tomography, finite element analysis and mechanical testing were used to guide the zoning process and printing parameters in order to manufacture consistent and robust capsule shell geometries. Additionally, dose consistencies of drug containing liquid formulations were investigated in this work.

1. Introduction

Drug product development can be a long and complex process especially when there is a need to: a) increase drug solubility by converting the form of the active ingredient through processes such as spray drying (SD) or hot melt extrusion (HME), b) protect the drug from a specific region of the gut using delayed release or enteric coating for release beyond the stomach or, c) alter the drug release profile to avoid adverse outcomes or overcome pharmacokinetic restrictions using modified or controlled release technology such as osmotic tablets. For each of these examples, the development of the dosage form becomes complicated, time consuming, and expensive. However, 3D printing (3DP) can allow for a robust, facile, and cost-effective approach to drug development in which drug release profiles may be tailored to a particular outcome using a single manufacturing method. Moreover, 3DP allows for custom designs and dosing amounts such that the dosage forms may be tailored to a specific patient population.

Fused deposition modeling (FDM) is the method of choice, where molten polymer is precisely deposited one layer at a time to build up a part. Currently, there are limited pharmaceutically acceptable materials available in filament form, which is the raw material feedstock for FDM printers. Many traditional polymer excipients do not have the appropriate thermal and mechanical properties for filament processing or the physical properties are altered when drug is incorporated in the filaments. In order to have a robust filament the polymer must be sufficiently rigid to maintain its form as it is pushed from the compression gear through the hot end nozzle orifice of the printer. The polymer should be sufficiently tough so the extruder gear of the FDM printer can gently depress and grip the filament to generate extrusion force greater than the resistance from the molten polymer flow out of the nozzle. In addition, the melting temperature or glass transition temperature must be significantly higher than the temperature inside the printing enclosure to allow the forced air cooling to rapidly quench the extrudate. The melting temperature should also be below 250 °C, which is the maximum temperature allowed in most commercially available FDM printers. Finally, in order to maintain proper molten flow, the thermoplastic material must not degrade while it is held at elevated temperatures during the printing process for extended periods of time, usually on the order of minutes. Once a filament is extruded, X-ray computed tomography (XRCT) can be used as a quality check for surface or volumetric defects (du Plessis et al., 2016; Markl et al., 2017). Diameter variations in the filament tend to strongly correlate with the

* Corresponding author at: 770 Sumneytown Pike, WP75B-110, West Point, PA 19486, USA.
E-mail address: derrick.smith@merck.com (D.M. Smith).

https://doi.org/10.1016/j.ijpharm.2018.03.056
Received 7 November 2017; Received in revised form 24 January 2018; Accepted 28 March 2018
Available online 29 March 2018
0378-5173/

quality of the final print as most commercial printers do not dynamically change the extrusion rate based on the filament's instantaneous diameter. Other challenges with this technology include the ability to extrude a tablet- or capsule-like product with good surface uniformity to encourage patient acceptance while limiting defect and internal cavity voids, as this influences active ingredient dissolution performance.

Over the past few years, there has have been numerous published references demonstrating successful fabrication of oral dosage forms using FDM. Hydroxypropyl cellulose (HPC) (Melocchi et al., 2015) has been used to print drug-free capsules which are manually filled and assembled post-printing. Additional work has highlighted the difficulties and limitations of using FDM for printing PVA capsules where the dosage forms were printed for hand filling with placebo liquids, followed by manual assembly and sealing, and external and internal surface roughness of the printed capsule walls were investigated. Typically, however, the filament that is loaded into the FDM 3D printer is pre-processed using extrusion to incorporate active ingredients, which are then used to print the final dosage form. Polyvinylpyrrolidone (PVP) (Okwuosa et al., 2017; Okwuosa et al., 2016) mixed with drug in a HME process has been used with FDM to construct oral dosage forms. Polyvinyl alcohol (PVA) has been most commonly used due to its beneficial mechanical and thermal properties aiding the FDM process (Goyanes et al., 2014, 2015a,b,c; Skowyra et al., 2015; Tagami et al., 2017; Markl et al., 2017). Recent work on manufacturing filaments for 3DP examined the use of Eudragit EPO®, a cationic acrylic polymer with dimethylamine-containing side chains, which is a polymer typically unsuitable for FDM due to its brittle properties (Sadia et al., 2016). This study showed that Eudragit EPO could be compounded with a plasticizer, triethyl citrate, and a non-melting filler, tricalcium phosphate, to optimize the hardness and flexibility properties to enable printing of the filament. The same research group demonstrated the feasibility of printing an enteric coated 3D printed caplet using the same plasticizer and filler approach with PVP and drug-free Eudragit EPO® (Okwuosa et al., 2017). Other extruded materials, where quinine was mixed individually with Eudragit RS, polycaprolactone, poly-L-lactic acid (PLLA), and ethyl cellulose at a 5 wt% drug loading, demonstrated viability for use as FDM filaments for preparing 3D printed implants (Kempin et al., 2017). It has also been demonstrated that soaking filaments in a poor or non-solvent solution containing drug can result in diffusion of drug into the filament, although the drug loading is intrinsically lower than extrusion methods (Goyanes et al., 2014). To date there are limited successful piloting examples of pharmaceutically acceptable filaments, and the surface quality of these printed dosage forms indicates more optimization is required before wide spread adoption can be realized. To sidestep many of these challenges, paste formulations have been printed using similar equipment as a FDM printer, except the hot end is replaced with a closed shot canister. Using this approach, Hydroxypropyl methylcellulose (HPMC) and polyacrylic acid (Carbopol® 974P), (Khaled et al., 2014) HPMC and lactose (Khaled et al., 2015a), and HPMC hydro-alcoholic gels (Khaled et al., 2015b) have been printed. Notably, this approach has been used for polypills, (Khaled et al., 2015a,b) which are single oral dosage forms that contain three or more isolated volumes each containing a different active ingredient. While paste formulations open doors to more material choices, this approach typically requires subsequent steps such as overnight drying of the print to remove any solvent or water from the dosage form for long term physical stability, it is unclear at this time how the mechanical robustness of paste printed dosage forms will endure secondary packaging and user handling.

In this work, the various challenges highlighted above are addressed with a new approach to manufacturing of pharmaceutical dosage: one-click FDM 3D print-and-fill capsules. We explore the idea and review the development work for a three step process integrated into a single FDM printer: 1) print an open faced capsule shell from a traditional polymer filament such that a formulation may be filled into the interior cavity, 2) fill the shell cavity with the desired dosage form, and 3) print the top of the capsule to close the opening for a fully sealed encapsulated oral dosage form. To accomplish this, the 3D printer files (.gcode) were modified through a process called zoning, where each individualized zone was printed with its own set of print conditions, namely extrusion rate, print speed, and quench rate. This zoning process eliminated macroscopic defects to the capsule shell and reduced sample to sample variation.

2. Materials and methods

2.1. Materials

Polylactic acid (PLA) 1.75 mm diameter filament by Gizmo Dorks (Temple City, CA USA) was used as a model polymer to establish appropriate conditions for regional slicing and print condition definition in these regions (so-called "zoning"). Polyvinyl alcohol (PVA) 1.75 mm diameter filament by Gizmo Dorks was used as the dissolvable capsule material. The PVA filaments were stored under high vacuum at 50 °C when not used and each filament spool was used for < 6 h at a time before re-drying overnight.

Metformin HCl salt (CAS 1115-70-4) was purchased from Uquifa (Cuernavaca, Mexico). Carboxy methyl cellulose (CMC, 90 kDa, CAS: 9004-32-4) and Polyvinyl alcohol (PVA, 6 kDa, 68% Hydrolyzed, CAS: 9002-89-5) were purchased from Acros Organics (NJ, USA). Hydroxyethyl cellulose (HEC, 90 kDa, CAS: 9004-62-0) was purchased from Sigma Aldrich (St. Louis, MO, USA). Polyethylene Glycol 400 Da (PEG 400, CAS: 25322-68-3) was purchased from TCI Chemicals (Portland, OR, USA). USP Grade Glycerin (CAS 56-81-5) was purchased from Procter & Gamble Chemicals (Cincinnati, OH, USA). All materials were used as received unless otherwise noted.

2.2. Capsule geometry

TinkerCAD (Autodesk, Inc.) was used to draw the capsule and exported as .stl files. Double concave tablet shaped capsules with a constant 10 mm diameter and 6 mm height were iteratively drawn and printed to optimize both the print quality and the visual familiarity of the printed capsules when compared to common pharmaceutical oral dosage forms. Deeper concave angles, or larger top and bottom taper angles, tended to more closely resemble familiar tablets, but deeper taper angles resulted in a more difficult to print shapes with a higher propensity for defects. The optimized geometry can be seen in Fig. 1a, and further details can be found in Section 3.1.

2.3. Design software and printer hardware

An as received Ultimaker 2+ (Geldermalsen, Netherlands) and a Hyrel 3D System 30 M printer (GA, USA) were used to print the capsules described here. The initial custom print method development (zoning) was done on the Ultimaker using PLA filament and the process was then tested for PVA. After establishing the process on Ultimaker, the process was transferred to the Hyrel 3D printer which had the capacity to use more than one filament and to integrate a syringe or other custom dispensing head for filling the capsules. PLA was used as a starting material due to its prominence in the 3D printing community and available literature to aid in optimizing the process for smaller dimensions. The Hyrel 3D printer was outfitted with a MK1-250 hot extruder head for use with the PVA polymer and stock 0.35 and 0.50 mm nozzles were CNC machined using our internal resources to optimize their geometry adjacent to the orifice. A custom designed 30 mL syringe head was used for filling the drug formulation on the Hyrel Printer (details can be found in the Supplementary Information). To print the capsules, Ultimaker and Hyrel print platforms were surface modified with 3 M blue painter's tape. To investigate the mechanical properties of the printed capsules, a 0.5 mm nozzle was also used on the Hyrel

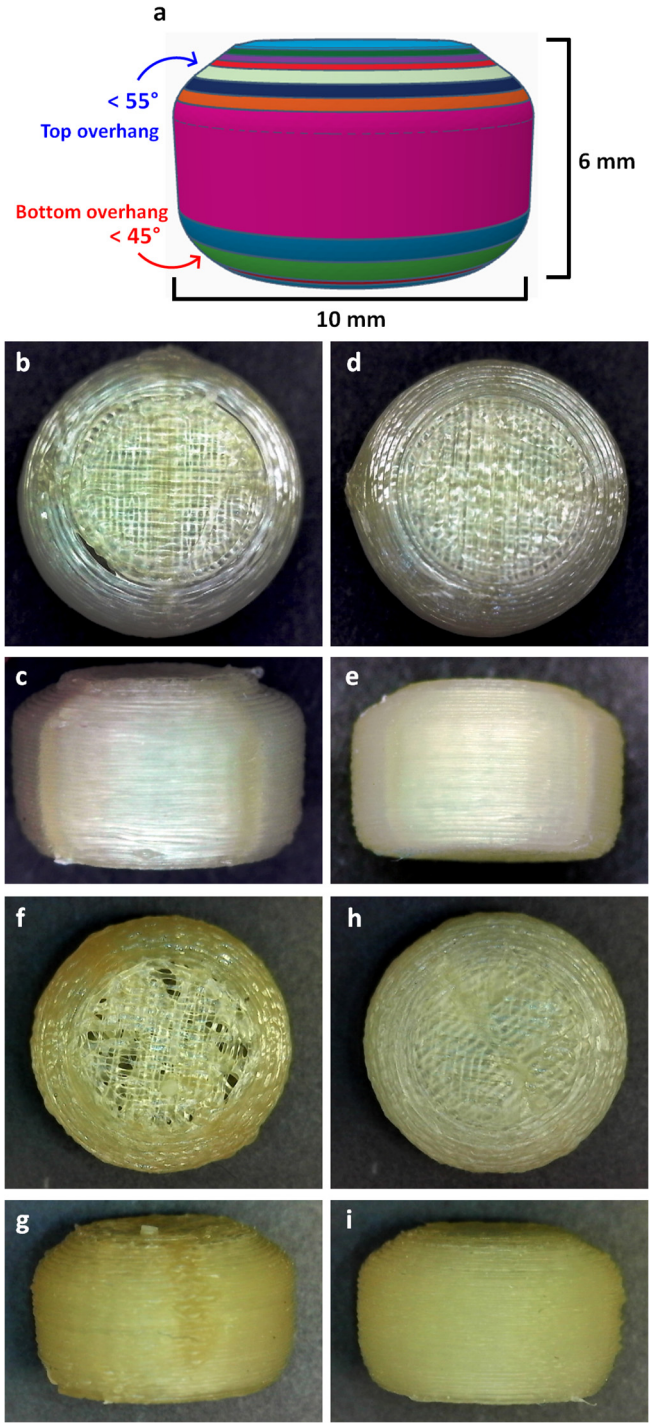

Fig. 1. (a) CAD representation of a single walled capsule with varying colors depicting the different print zones. (b, c) Top and side optical views, respectively, of PVA capsules printed on a Ultimaker 2+ at 60 mm/s with no zoning, and (d, e) with zoning. (f, g) Top and side optical views, respectively, of PVA capsules printed on a Hyrel 3D System 30 M at 25 mm/s with no zoning, and (h, i) with zoning.

printer to change the layer-layer overlap, which is described in more detail in Section 3.3.

Beyond the hardware modifications described above, significant effort was also made to address the software that controls the FDM printer. Typically in 3D printing, the object to be printed is processed through an algorithm that slices the object into defined layer heights that prescribes the path for extruder and the parameters for extrusion into a file known as 'gcode'. The gcode file also instructs the printer to control the temperature of the nozzle and the platform, and controls the fan used to facilitate the quenching of hot polymer. In this work, the .stl files (see Section 2.2) were imported into Cura v15.04.06 for slicing and conversion to a gcode. The layer height for the capsules was 0.15 mm unless otherwise noted. Since the capsule walls were only 0.4 mm thick, no infill was used in these prints, and thus no infill raster angle was used. The bottom two and top 3 layers of the capsule used a rectilinear fill, where a given layer was offset by 90° to the previous layer. The extruder head velocities used on the Ultimaker printer were 80 mm/s with the exception of the first layer which was set to 40 mm/s, with travel speeds of 150 mm/s. The Ultimaker's print platform was set to 60 °C with an extrusion temperature of 200 °C for PVA, and between 200 °C and 230 °C for PLA. When our work transitioned to the Hyrel the print speeds were reduced to a maximum of 25 mm/s for all prints and travel moves due to the increased weight of the print head assembly which limits the maximum acceleration. The Hyrel's print platform was set to 30 °C with an extrusion temperature between 180 and 206 °C for PVA. Slower printing speeds on the first printing layer increase the adhesion between the printed object and the print platform; to maintain a relatively consistent bed adhesion, the platform temperature used on the Hyrel was reduced.

2.4. Print zoning and tool change code

The zoning process developed here divided the .gcode into separate printing regions, or zones. These zones were chosen based on the geometric features of the capsule, such as the overhang angle of the walls. Each of these zones was given separate printing conditions to optimize the print quality for that specific zone, which is outlined in more detail in Section 3.1. The final divisions within the .gcode, or the different zones, are depicted in Fig. 1. Single-walled prints were 6.0 mm high, which translates to 40 layers for 0.15 mm layer heights. In total, there were twelve zones. The bottom two layers in contact with the printing platform were the first two zones. The next two zones are comprised of the bottom concave portion of the capsule. The vertical wall portion is the next print zone. The next two zones after the vertical capsule wall are the top portion of the overhang followed by the layer just preceding the capsule filling step. This filling step, where the active ingredient is loaded into the capsule shell, is handled as a tool change with custom gcode (see Supplementary Information). In general, the ability to control the volumetric dispensing of our formulation depends on the tolerance of the positioning screw and the volume of the syringe used to hold the formulation. The last four layers, which is the final 0.6 mm of the capsule, are treated as individual zones and used to enclose the capsule after the filling step. With the exception of the bottom layer and the layer subsequent after the filling sequence, the print speed remained constant, and only the fan speed and extrusion rates were modified. For the first layer after the filling, the print speed was reduced to 30–50% and fan speed was either reduced or turned off to assure good mechanical adhesion.

2.5. Physical characterization

Optical images were captured with a Plugable USB 2.0 (WA, USA) digital microscope with a resolution of 640 × 480 pixels. A Bruker Skyscan 1275 X-ray microcomputed tomography (XRCT) system (Belgium) was used to observe inter and intra-layer quality and defects, internal scaffolding geometry, and any other overall defects on the surface or inside the walls of PVA capsules. Empty capsules were scanned with the following settings: 35 kV, ~266 μA, ~130 ms per image, 20 frame averages, and 0.08 or 0.10°rotation between images over 360 degrees of rotation.

2.6. Mechanical testing

Mechanical strength of the capsules was tested in shear using a Dr. Schleuniger Pharmatron Tablet Tester Model 8 M (Aesch, Switzerland) with a 400 N load cell. A constant displacement rate in the tester was maintained at 1 mm/s. The capsules were loaded into a custom shear plane fixture with a 3D printed spacer of 2.90 mm to test the same shear plane from sample to sample. The peak force to initial failure is reported in this work. Peak force here is the maximum compression force recorded while shearing the sample. A schematic of the fixture used is shown in the Supplementary Information.

2.7. Fill preparation

Polymeric fills for the 3D printed capsules were prepared by using a Thinky ARE-310 (Thinky USA, CA) high shear mixer. The requisite formulations were measured in a 20 mL vial and mixed for 10–30 min at 2000 rpm. All measurements were done on a weight basis and the drug concentration was kept constant across the formulations at 15 wt%. In most cases, the polymer and drug dissolved within 10 min and where it did not, the system was allowed to mix until a clear solution was obtained for a maximum of 30 min. For the PVA and HEC fills, the wt% noted is for the polymer (Fig. 6), with 15 wt% Metformin (rest water). The glycerin + CMC fill was 15 wt% Metformin, 2.5 wt% CMC, 20 wt% PEG 400, 27.5 wt% glycerin, and 35 wt% water.

2.8. Viscosity measurements

Viscosity was measured using ARES G2 (TA Instruments, DE) at room temperature using a cone (50 mm cone with an angle of 0.04 rad) and plate geometry. A flow sweep method was performed using shear rates from 10 s^{-1} to 100 s^{-1}.

2.9. Finite element analysis

ABAQUS 2016 (Simulia – Dassault Systèmes), a finite element software package, was used to optimize the capsule geometry by estimating relative differences in the maximum principal stresses generated during swelling as a result of moisture absorption of the capsule shell from the liquid formulation. Due to the fundamental similarities in the governing equations between moisture and thermal diffusion, moisture uptake was modeled using thermal analysis. On the interior of the capsule, which would be exposed to the waterborne filling, a fixed temperature was imposed at the beginning of the simulation and remained constant throughout. This constant thermal boundary condition is analogous to the polymer instantaneously reaching equilibrium saturation when in contact with the waterborne filling. The exterior of the capsule was considered insulated where heat transfer would not occur beyond the outer surface to emulate the condition of no moisture flux out of the capsule exterior surface. Each capsule was meshed with quadratic tetrahedral elements with thermal and kinematic degrees of freedom. The polymer was modeled as an elastic material with a Young's modulus of 1.2 GPa and a Poisson's ratio of 0.35, similar to that of reported values for a PVA material (Mohsin et al., 2011). Thermal conductivity was set to 10 W/m·K, material density was set to 1540 kg/m^3, specific heat was set to 1000 J/K, and thermal expansion was set to 1/1000·K. For simplicity, residual stresses likely inherent from the print process were ignored for these simulations. The initial temperature of the system was set to zero degrees (no initial moisture content) and the entire interior surface was set to one degree at time zero. This boundary condition equates to an instantaneous step change in the surface concentration of the interior of the capsule. The simulation was run to thermal equilibrium and stresses were analyzed during the time to reach equilibrium.

3. Results

3.1. Custom print procedures

To determine the optimal conditions for 3D printing our model polymer (PLA), numerous slicing and print parameters were explored using the Ultimaker 2+ . Of interest in this work and for our specific clinical application was the minimization of dosage form print time in order to facilitate effective utilization of this technology to be considered an on-site formulation approach. Print speeds near the printers' maximum velocity were started with, and then further processes optimization focused on print quality, which we believe is strongly correlated to print defects. Before detailing these parameters, the following terms are defined. Print speed is the speed at which the print head moves while depositing molten polymeric material. Extrusion rate is the amount of polymer filament pushed through the hot end during printing, relative to the amount of material the slicing software calculated to fill the volume in each slice. For example, an extrusion rate of 200% would imply that twice the amount of material is extruded than was calculated by the slicer to fill the selected volume. Bridging is a phenomenon that occurs when a hot end nozzle must extrude material from one structure to another in an unsupported manner. In this case, the first layer of the top of the capsule (red layer in Fig. 1a) is a bridging layer. Fan speed refers to the speed of the fan oriented at the printed capsule directly under the hot end nozzle. Fan speed is typically given as a percentage and requires anemometer calibration for an accurate measurement of airflow determined by the power of the fan and the air duct geometry.

For printing the capsules using PLA on the Ultimaker 2+, it was determined that a fan speed of 70% (which corresponds to 4.0 m/s air flow measured at the nozzle), nozzle temperature of 210 °C, and a platform temperature of 60 °C were optimal for print speeds between 60 and 80 mm/s. Additionally, a maximum layer height of 0.15 mm allowed for excellent capsule surface uniformity under visual examination with a print time of 84 s for each capsule shell. Iterative design on the capsule geometry enabled us to optimize the curvature on the top and bottom tapers for adequate platform adhesion and minimal defects in bridging. As shown in Fig. 1a, for layer heights of 0.15 mm and a nozzle with a 0.35 mm orifice, the bottom taper angle needs to be $< 45^{\circ}$ offset to the bed's normal, and the top taper angle needed to be $< 55^{\circ}$. To generate a more familiar tablet-like image and visual elegance, a spheroid shape was used for gradual curvature on the sides, followed by a conical shape once these critical angles were established. In Fig. 1a, the top taper section of the capsule can be divided into two parts: the spheroid shape in the top portion of the pink zone, and orange and dark blue zones; and the conical shape, comprised of the light green zone and the zones above it. Some general printing parameters were determined during this zoning process: (1) bottom layers of the capsule were purposely over-extruded at 180% for the first layer and 105% for the second; (2) zones below the vertical pink zone would gradually decrease in extrusion rates such that the pink zone was printed with extrusion rates of 95–100%; (3) extrusion rates above the pink zone would again be increased to 108–115% before the formulation filling sequence initiation; (4) in the layer just after the filling sequence (red zone in Fig. 1a), the print speed was reduced to 30–50% with a significantly reduced air flow rate (15% fan speed) and an extrusion rate of 120% to promote inter layer adhesion; (5) the outer perimeter on the first bridging layer was printed with the same parameters as zone (4) but the inside and unsupported perimeter layer was printed with a fan output at 100% (roughly 4.7 m/s) to reduce the potential of printed filament sagging; (6) the last two layers of the capsule were extruded at a rate of 125–150% to assure significant layer overlap and an adequately sealed top

The zoning parameters used for PLA discussed above were used as a starting point for our work with PVA on the Ultimaker 2+, with the nozzle temperature set to 200 °C, platform temperature of 60 °C, fan

speed to 15% (roughly 1.8 m/s) and print speeds of 60 mm/s for single wall prints. At zone (5) where the layer has bridging, the fan speed was increased to 45% to increase the quench rate and reduce the potential for sagging of the printed filament. It should be noted that increasing print temperatures beyond 200 °C were shown to improve mechanical properties of the PVA capsules but at a cost of more frequent nozzle fouling due to PVA thermal degradation. Using a maximum temperature of 200 °C and a print speed of 60 mm/s, nozzle integrity for at least 50 cumulative hours of printing is achievable. Further discussion on the relationship between print speed and extrusion temperature is detailed in Section 3.3. The impact to capsule quality as a result of the appropriate use of 'zoning' can be seen in Fig. 1b–e. Fig. 1b and d show a PVA print at 60 mm/s with no zoning. In this example there are two critical failures in the resultant capsule. First, large pores are present at the top of the capsule, which include both the layer after a tool change, and also one to two layers prior to the tool change. Fig. 1d shows a sagging bottom taper layer, resulting in weak layer-layer bonding. This is due to insufficient material extrusion and surface area available for bonding to previous layers. This phenomenon is exaggerated at higher taper angles near the bottom where subsequent layers are greatly offset from the previous layer. Fig. 1c and 1e demonstrate that the zoning process eliminates these failures. These same parameters were transferred to the Hyrel 3D System 30 M printer. The Hyrel 3D System 30 M printing was limited to a maximum speed of 25 mm/s due to the increased mass on the print head and limitations on the motors and belts driving the motion. As a result, capsule shell print times increased to about 3.5 min. It is known that at slower print speeds, part uniformity and mechanical integrity increases(Christiyan et al., 2016); however, failures were still observed at this speed on the Hyrel 3D System 30 M, as shown in Fig. 1f–i. The failure mode in this case is inadequate printing of the top layers leaving pores in the top of the capsule. The zoning process eliminated these pores, as well as increased the surface quality of the capsule. To this end, the zoning process was demonstrated to eliminate macroscopic part defects and increase surface uniformity on the 3DP capsules with two distinct materials on two separate printers.

3.2. Scaffold design: Finite element analysis

One critical failure that was identified in our work was the integrity of the layer to layer adhesion whereby poor bonding would result in dissolution variability and possible "dose dumping" and/or formulation leakage, which is undesirable and a potential safety risk to the patient. After a capsule is filled with a water-based formulation, moisture ingress into the PVA capsule walls results in swelling of the walls. This swelling leads to complex stresses within the capsule walls, and if the layer adhesion is not sufficient, a delamination failure mode is likely to occur and was observed in our initial capsule designs.

In order to minimize the likelihood of layer delamination, but keep the overall capsule geometry fixed, finite element analysis was used to understand how changing the scaffold geometry affected macroscopic stresses as a result of swelling. Without the structural support of the scaffold, the bridging layer sags and several extra layers would have been required to seal the top of the capsule. Since the scaffold is necessary to print a top with comparable thicknesses to the capsule base and walls, an optimized scaffold design should result in a structure that does not increase swelling while allowing for sufficient support to finish the printing of the top of the capsule.

Numerical swelling experiments were performed on two different scaffold designs: a two-fin and a four-fin scaffold design. The four-fin and two-fin scaffold capsule geometries are shown in Fig. 2a–d. The images in Fig. 2a–b are 3D CAD renderings of the geometry with the capsule walls translucent such that the internal scaffolds could be seen. Images in Fig. 2c–d are cross sections through the center of the four and two wall scaffold, respectively. This analysis provides a means to compare the relative magnitude of tensile stresses generated during swelling between the two scaffold geometries. Residual stresses as a result of the printing process were ignored for this analysis and the stresses generated were solely due to swelling strains. The omission of residual stresses allowed for a more direct comparison between scaffold geometries. For a more realistic model of the swelling phenomenon, the incorporation of residual stress would be necessary, but was not required for this study.

The resulting maximum principal stresses were analyzed at the same time point during the swelling processes. Fig. 2e shows the maximum principal stresses on the exterior surface of the capsule upon swelling for the four-fin geometry. Two regions of stress concentrations arose during the experiment: 1) at the center of the top layer, and 2), at the intersection of the capsule wall and each of the scaffold fins, roughly perpendicular to the center of the long side of the fin scaffold. These stresses are caused by the scaffold fins. Since the scaffold fins are exposed on both sides of its walls to the water-containing fill, they will swell faster than the capsule wall, which only has the internal side of its walls exposed to the water-containing fill. The first stress concentration is caused by each of the four fins swelling faster than the outer capsule shell, and pushing against each other at their central intersection, out towards the side walls in all four directions. Due to the orientation of the extrudate, being in-plane to these swelling-induced stresses, this stress concentration should not significantly induce delamination. However, the stress concentrations at the connection between the scaffold fin and capsule wall are oriented such that their normal stresses, with respect to each printed layer, are significant, and will result in delamination if these normal stresses exceed the layer-layer bonding strength.

To address these stress concentrations, a second two-fin scaffold design was evaluated based on the four-fin scaffold results, (Fig. 2b and d). The key design principle is to minimize the volume of the scaffold structure while maintaining its ability to prevent upper layer sagging. A two fin design was chosen so that less scaffold material would push outwards against the capsule shell when swelled, limiting the stress concentration in the top center of the capsule. For the same reason, the two scaffold fins were modified so there was a 0.2 mm gap at the center, eliminating their ability to directly push off one another when swelled. To reduce the swelling-induced stress concentrations along the connection between the scaffold fin and outer wall, the overall size of the fins were greatly reduced. Fig. 2f shows the resulting stress concentrations with the modified two-fin scaffold geometry. Interestingly, despite modifying the fins such that they could not push against each other outwards against the capsule walls when swelled, there was a slight increase to the stress concentration at the center of the top of the capsule. The majority of the top of the capsule, however, showed a reduction to swelling stresses. More importantly, the region where the stresses, normal to the printed layers' plane, showed a reduction to swelling-induced stress concentrations, from 75 kPa for the four-fin to 60 kPa for the two-fin scaffold. These stresses were also distributed over a smaller area for the two-fin scaffold. Additionally, this region is more likely to fail due to delamination because of the reduced contact area between layers; further supporting, the two-fin scaffold geometry to be more mechanically robust under swelling conditions. The two-fin scaffold geometry was used for all capsules hereafter. Consequently, the finite element analysis provided a means to optimize scaffolding supports needed to eliminate delamination defects.

3.3. Print defects

For this process to be considered viable in the pharmaceutical industry, understanding print to print variations is critical because defects or inconsistencies in the prints could lead to a high variability in drug product dissolution. The most influential parameters dictating print quality were print speed, nozzle temperature, and fan speed. High fan speeds resulted in prints that could be easily delaminated on handling, indicating the layer-layer healing during the printing process was not sufficient. Thus, the lowest fan speed (15% or 1.8 m/s) to print a non-

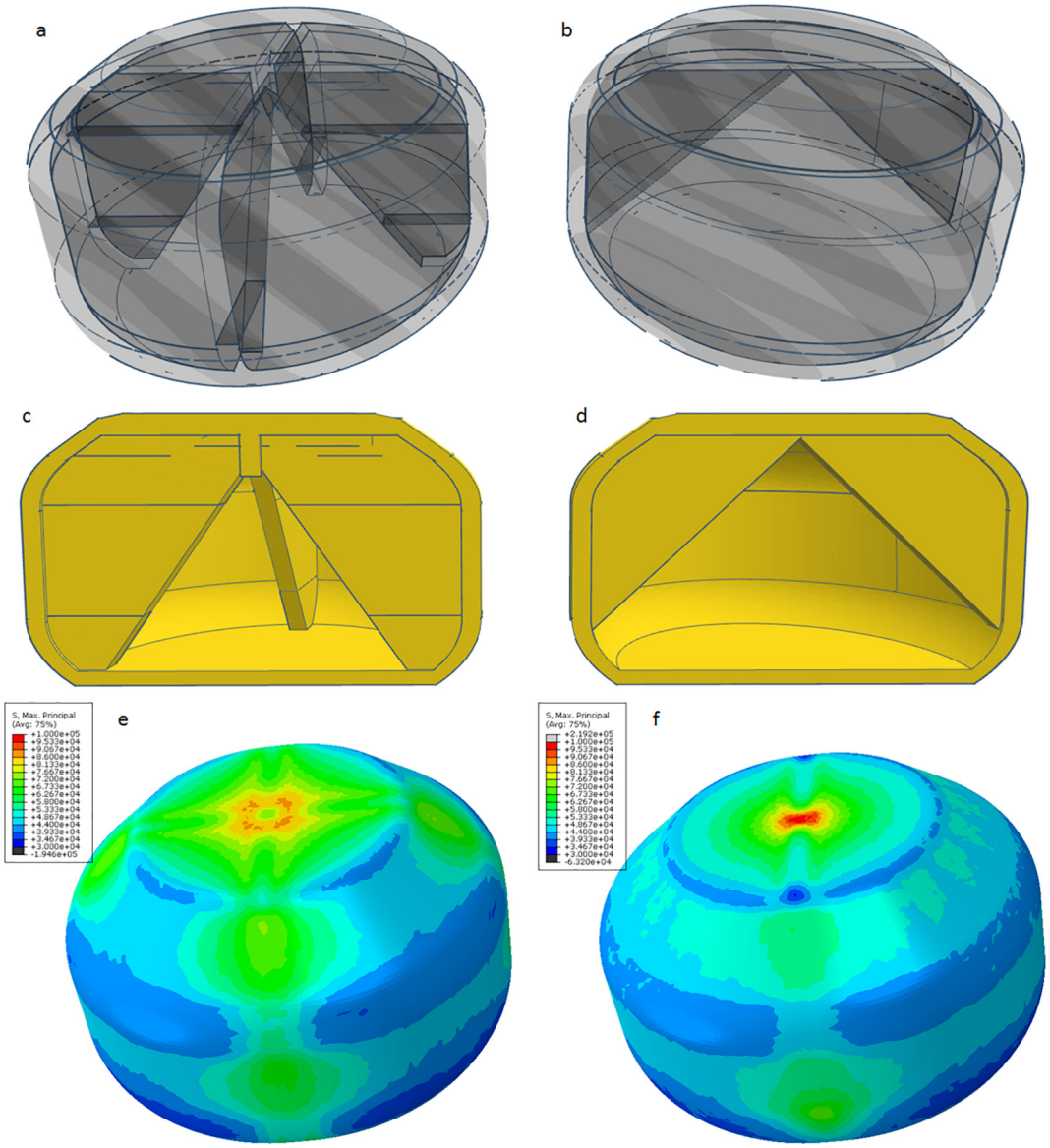

Fig. 2. (a, b) CAD image of a 4-fin and 2-fin scaffold design in a translucent rendering, (c, d) side-view with a cut out to show fin shape, (e, f) and an image taken of a finite element model at a critical time point showing the variation of potential internal stresses from moisture swelling. The scale bars (e, f) are 3.00×10^4 Pa (black) to 1.00×10^5 Pa (red). (For interpretation of the references to colour in this figure legend, the reader is referred to the web version of this article.)

sagging scaffold and shell structure was used to maximize part healing, or layer-layer bonding. The nozzle temperature and print speed correlated with each other due to polymer degradation kinetics and dwell time within the print extruder. When PVA degrades, it tends to crosslink (Futama and Tanaka, 1957), which causes build-up in or around the nozzle, reducing the intended molten flow, or the nozzle orifice area, or both. Maximum sustainable extrusion temperatures with a 0.35 mm nozzle were empirically determined at various printing speeds, shown in Fig. 3. The maximum sustainable temperature refers to the maximum temperature that could be used over the course of at least one month of daily use without seeing nozzle clogging failure due to polymer degradation; temperatures above this would result in clogged nozzles from degradation of the PVA over time, indicated in red. The yellow and red regions at fast speeds and low temperatures indicate conditions that result in poor mechanical properties. In addition to temperature and speed, the layer-layer overlap at the largest overhang angle was increased in two ways. First, a 0.50 mm nozzle was used, maintaining the same layer height. Second, the 0.35 mm nozzle was kept, but the layer height was reduced from 0.15 to 0.10 mm only in the top region of the capsule where there was a steep overhang angle. A scheme of these changes can be seen in Fig. 4d. From the 0.35 mm nozzle data, the material flow rate was calculated using the layer height, print speed, and path width of the nozzle, and this was used to calculate and extrapolate the print speeds to use for the 0.50 mm nozzle at each temperature. For instance, the print speeds and temperatures for the 0.50 mm nozzle were 15.4 mm/s at 198 °C, which matches the flow rate for 22 mm/s with the 0.35 mm nozzle, and 22 mm/s at 206 °C. It should be noted that this print speed and extrusion temperature relationship is unique to PVA, and may not translate to other polymers.

Defects were macroscopically assessed by mechanical shear testing with an understanding that larger size and population of defects will result in higher variability in the peak shearing force. To further evaluate the impact of print speed, additional conditions were tested for this analysis so that the top overhang zones have a layer height of 0.10 mm, shown in Fig. 4a–b. This was to increase the layer-layer overlap and decrease the tapering effect. The results of the mechanical shear test are shown in Fig. 4c. There are three notable trends: 1) as temperature and print speed are increased, the required force to break the capsules

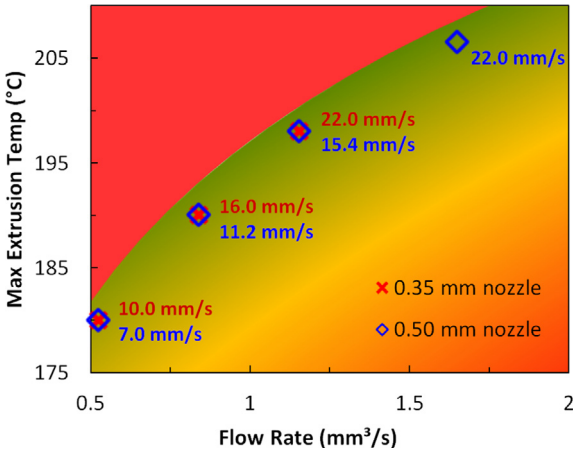

Fig. 3. Graph of flow rate versus maximum sustainable extrusion temperature on a Hyrel 3D System 30 M printer. The red region above data points indicate conditions at which the nozzle will clog due to PVA degradation. The red region in the bottom right corner indicates poor print conditions resulting in poor mechanical properties of the printed capsule, or non-flow through the nozzle orifice. The green region indicates a stable print condition with better mechanical properties. (For interpretation of the references to colour in this figure legend, the reader is referred to the web version of this article.)

increases. Print speeds of greater than 16.0 or greater than 15.4 mm/s for the 0.35 and 0.50 mm nozzles, respectively, result in saturation of the mechanical strength. 2) There is a significant softening of the capsules from ambient laboratory humidity (between 20 and 30% relative humidity) when stored on a bench top for more than 24 h, but the capsules are mechanically unaffected by moisture for at least 4 h. 3) Increasing the layer-layer overlap significantly reduces the capsule-to-capsule variation.

X-ray microcomputed tomography (XRCT) was performed on the capsules to observe the spatial uniformity and morphology of the prints. The 3D rendering of reconstructed images of the capsules printed at various conditions are shown in Fig. 5. For both nozzle thicknesses used in this work, slower printing speeds results in a more uniform internal and external surface roughness. As print speed increased, the surface roughness increased. It should be noted that at the highest print speed (22 mm/s) with the 0.50 mm nozzle, macro voids were observable (images can be found in the Supplementary Info), suggesting this may be nearing the maximum polymeric flow rate for PVA using this nozzle diameter. For the 0.35 mm nozzle with all 0.15 mm layer heights in Fig. 5a–c, there is a tapering of the wall thickness towards the top of the capsule as the wall approaches the top cap. In an attempt to keep the wall thickness constant, the layers in the top overhang area were decreased to 0.10 mm heights, shown in Fig. 5d. Decreasing the layer height in this zone significantly decreased the tapering effect, particularly on the 3 layers before the bridging layer. For the 0.50 mm nozzle prints with 0.15 mm layer heights, shown in Fig. 5e–h, this tapering effect of the top overhang was reduced for the 15.4 and 22.0 mm/s prints, and not observable for the slower prints at 7.0 and 11.0 mm/s. The same procedure of reducing the layer height in the top overhang zone was performed on the 15.4 mm/s print, shown in Fig. 5i. Reducing the layer height eliminated any observable tapering effect. Additional views can be seen in the Supplementary Information. The optimum conditions carried forward were using the 0.35 mm nozzle, with print speeds of 16 mm/s, nozzle temperature of 190 °C, top layer height as 0.10 mm.

3.4. Fillings characterizations

Viscous liquid and gel fill formulations with various viscosities were prepared to analyze the printer's capabilities of filling the capsules.

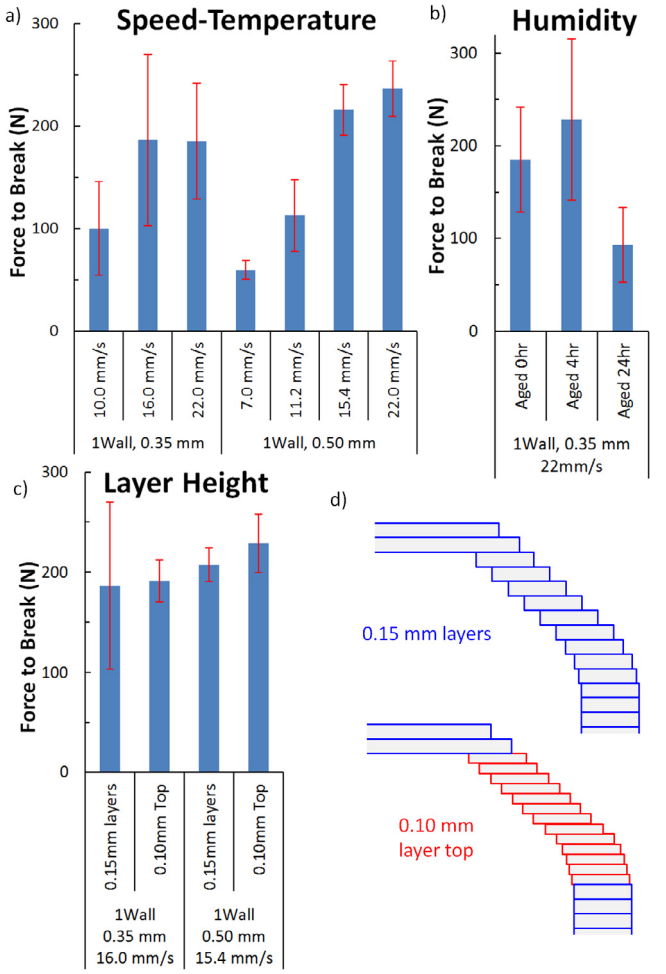

Fig. 4. (a) Graph of force required to shear to failure capsules printed at various combinations of speed and temperature for 0.35 or 0.50 mm orifice nozzles, (b) printed at a static condition of 22 mm/s at 198 °C with a 0.35 mm orifice nozzle and aged in atmospheric conditions, (c) and two print conditions with two top overhang layer heights, 6 replicates per set. (d) Schematic of top overhang layer heights for a global 0.15 mm layer height and with a local 0.10 mm layer top overhang, not drawn to scale.

Viscosity was measured on the fill formulations to quantify their printability. The main criterion for determining if a formulation was viable was to check if the formulation dripped during the printing of the capsule. In all cases the drug concentration was fixed at 15 wt% and the polymer concentration was increased to improve the viscosity of the formulation which allowed for continuous manufacturing of the 3D printed tablet. Fig. 6 shows the viscosity of various fills that were prepared for this work, where the red bars indicate a failed system due to formulation drip during the print. When not actively injecting, the syringe head would retract the fill formulation as much as possible without drawing bubbles into the syringe head. This was to minimize any drips that might fall out of the syringe needle while the head assembly is jolting around during the FDM printing process. This also served to minimize any evaporation of the water in the fills during the printing process. Formulations under 50 cP were tested with both 18 and 21 gauge blunt needles, and it was observed that the needle gauge in this range had no observable effect on whether or not the formulation would drip during printing. To avoid any dripping from the blunt needle during the printing process, the viscosity was formulated to be greater than 20 cP.

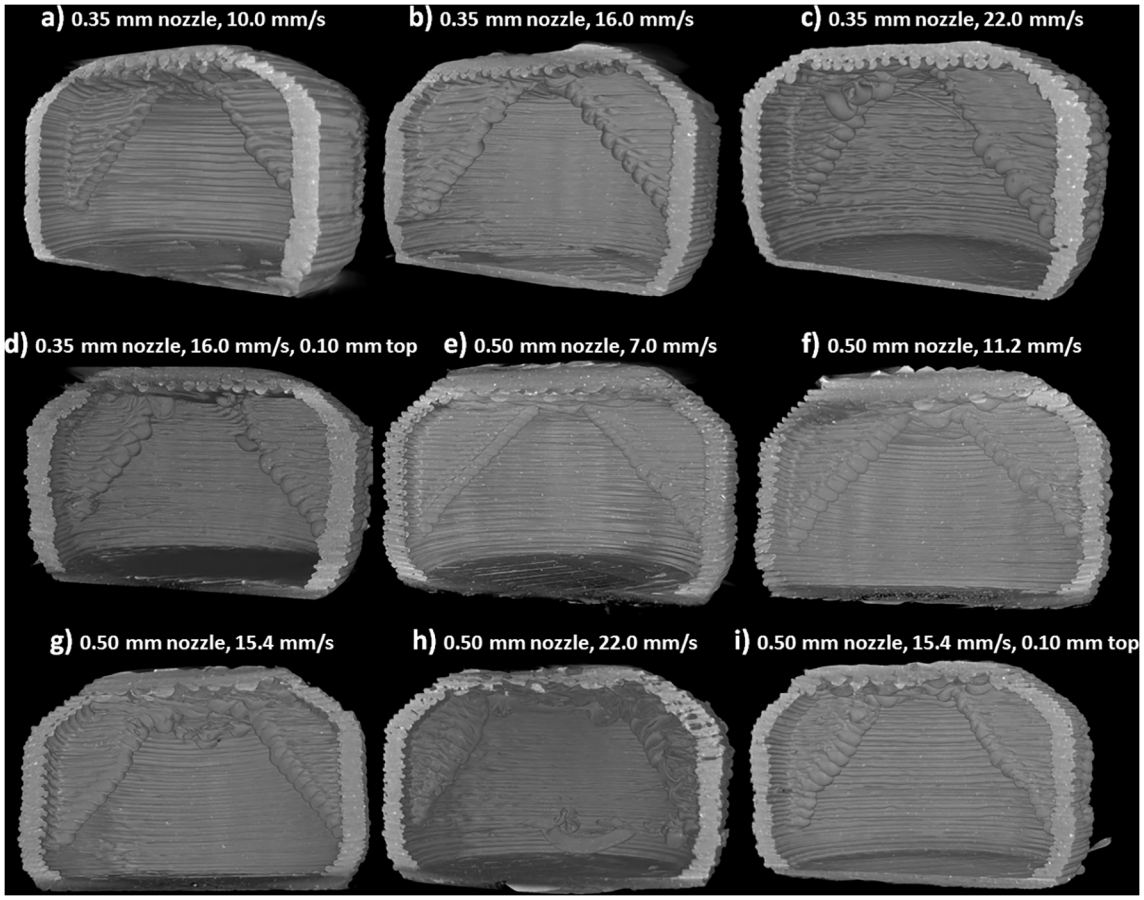

Fig. 5. XRCT reconstruction images of capsules with various print conditions on a Hyrel 3D System 30 M printer, cropped to see the internal wall structure and shape.

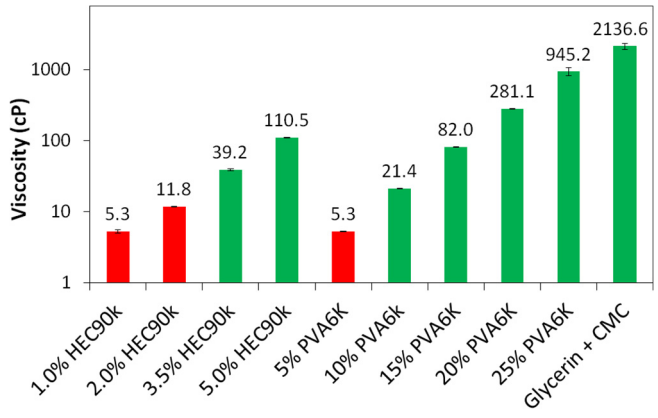

Fig. 6. Viscosities of various water containing fillings. Red indicates the viscosity was too low for a 20 gauge blunt syringe during the printing process, resulting in dripping from the syringe; green indicates the filling is printable. (For interpretation of the references to colour in this figure legend, the reader is referred to the web version of this article.)

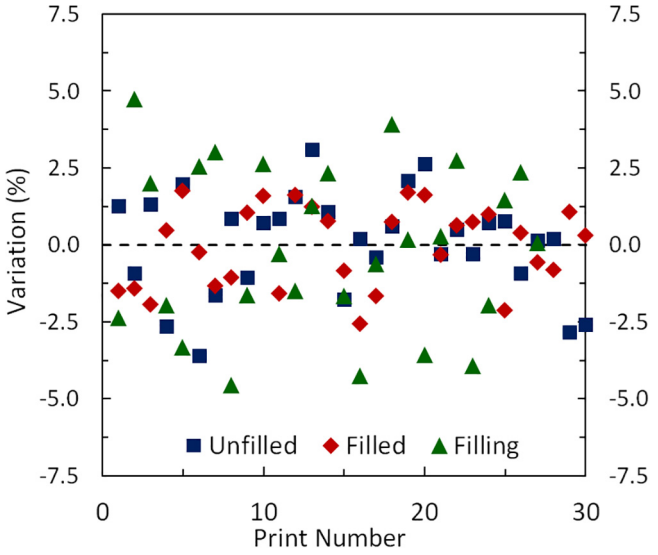

Fig. 7. Variation with respect to average print weight of 30 prints for unfilled capsules (blue squares), capsules filled with HEC filling (red diamonds), and HEC filling shots into a vial (green triangles) on a Hyrel 3D System 30 M printer. (For interpretation of the references to colour in this figure legend, the reader is referred to the web version of this article.)

3.5. Printing repeatability

Of importance was determining the repeatability of the printing process, capsule visual uniformity, reliable encapsulation, and consistent formulation injection mass. Details on the custom filling sequence gcode can be found in the Supplementary Information. To test the 3D printing repeatability the Metformin gel formulation with 3.5 wt % HEC was used. 30 prints each of unfilled capsules, drug formulation-filled capsules, and an external drug formulation injection were weighed, shown in Fig. 7. For all three print sequences, the variation was within ± 5% of the average weight. The coefficient of variation for the unfilled and filled capsules, and filling were 1.66%, 1.31%, and 2.72%, and the process capability indexes were 1.00, 1.28 and 0.61, respectively.

4. Discussions

A novel approach using FDM 3D printing is demonstrated for preparing drug dosage forms. In this manuscript liquid filled capsules have been covered, but the approach can be translated to a variety of other fills materials such as pastes and particulates. As demonstrated here, printing well controlled thin walled capsule shells out of pharmaceutically acceptable materials requires significant re-engineering of gcode for high quality dosage forms on the order of commonly manufactured capsules. The expected mechanisms underlying dissolution profiles of custom designed capsules will be somewhat different from classic dosage forms. Gelatin capsules quickly dissolve and expose the filling to the gastro-intestinal tract, and tablets either erode to slowly expose fresh drug on the surface or disintegrate to rapidly release the active ingredient. This work proposes the use of 3DP capsule design, geometry, and material with control over the release timing of the fill. It is expected that the shear velocity of dissolution medium will modify the release profile, as has been demonstrated with other PVA-based systems.(Morita et al., 2000) Additionally, it is expected any collection of defects in the 3D printed capsule that would sacrifice mechanical integrity once the capsule is swelled, will play a critical role in the drug release rate and repeatability. Specifically for water rich fills, using tools such as FEM will enable a better understanding of the inherent internal stresses within the capsule at equilibrium, especially for short or long-term packaging. On-going work includes the investigation of the dissolution mechanisms on these PVA 3D printed capsules.

The first use of mechanical tests can be used to better understand the construction of the layers and interfacial strength and draw correlations between various print parameters and capsule integrity. From the testing on these capsules it can be seen that the mechanical properties vary greatly under different print conditions. Starting at lower temperature-speed combinations, less shear force is required to break the PVA capsules. Once the 190 °C temperature-print speed combination is reached for either a 0.35 or 0.50 mm orifice nozzle, the boost to mechanical properties plateaus. While printing the slowest speed tested here provides a uniform surface, reduced mechanical properties could cause the capsule to be prone to delamination under rough handling conditions, or possibly from swelling during dissolution. Since faster print speeds generally results in a rough surface, a print speed near 16 mm/s appears to be a local optimum for mechanical properties and print uniformity for these PVA capsule shapes in the Hyrel printer. A second use for mechanical properties is looking at print to print variability. Quantifying the print variation from sample to sample is critical for repeatable results in other testing, notwithstanding dissolution. It was observed that increasing the layer-layer overlap by increasing the nozzle orifice diameter, or by decreasing the layer height, decreased the failure force variation, indicating that the defect concentration was reduced. The results of the shear test may also help discriminate for features too small to be observed with the resolution of the XRCT scans such as micro-void defects, or regions of layer-layer contact areas that did not sufficiently bond. Reducing the defect concentrations may also reduce the variation in dissolution, since a collection of void defect along a layer-layer interface may cause faster erosion and dissolution along that plane, prematurely bursting the capsule. One caveat to these results, due to the print speed and extrusion temperature relationship realized for PVA printing to be stable, is that temperature may not always be the dominant factor in mechanical strength over print speed. Each material may behave differently; however, both print speed and extrusion temperature may be important parameters to optimize to manufacture mechanically robust capsules. Tests such as mechanical shear could also be used as an on-site quality measure to ensure that clinical batches manufactured at a remote site meet specification.

The liquid filled capsule industry has paved the way for a large pallet of excipients to potentially dissolve any BCS Class I and III drug, and here it is demonstrated that a variety of fillings containing 15 wt% drug of a BCS Class I drug did not drip during FDM printing, and thus were amenable to 3DP technologies. We are currently investigating various liquids and automated alternate materials dispensing technologies that can incorporate into current 3D printing technology to increase the range of applicable filling types to readily be used in capsule printing.

5. Conclusions

Custom hardware and software 3D printing methodologies were applied to an open-sourced 3D printer (Hyrel 3D System 30 M) in the development of FDM 3D printed oral dosage forms with excellent visual uniformity. In this work, software modifications to the 3D printers operating instructions (.gcode) has demonstrated the ability to decrease print to print variation, decrease wall thickness variation within the capsule, and construct single walled features that are able to be filled with a drug containing formula within a single operation. Mechanical testing and XRCT were successfully utilized to observe the impact of print conditions on mechanical strength, surface and volumetric defect population, as well as the influence of layer-layer overlap for high angle overhangs and its role in print uniformity and repeatability. Drug containing liquid fills were formulated, and corresponding hardware modifications to the apparatus controlling the syringe used to dispense the formulation were developed to enable seamless and straightforward printing of these thin-walled capsules filled with drug with acceptable repeatability. Overall, we have successfully demonstrated how the FDM technique can be creatively used to prepare dosage forms where the API is not exposed to harsh conditions during FDM, and which can be tailored by changing the FDM capsule on demand. By developing this approach, we believe we will be able to use this 3D printing platform for rapid on-site formulations. Our current work is focused on developing appropriate dissolution methods for these 3D printed drug delivery systems which have tunable release profiles.

Acknowledgements

The authors would like to thank Joe Rock from the Merck & Co., Inc. Design Center in West Point, PA, USA for aiding in nozzle machining and Gary Kowalski from the Merck & Co., Inc. Device Development group in Rahway, NJ for replicating PTFE nozzle components.

Author Disclosure Statement.

No competing financial or personal interests exist.

Appendix A. Supplementary data

Supplementary data associated with this article can be found, in the online version, at http://dx.doi.org/10.1016/j.ijpharm.2018.03.056.

References

Christiyan, K.G.J., Chandrasekhar, U., Venkateswarlu, K., 2016. A study on the influence of process parameters on the Mechanical Properties of 3D printed ABS composite. IOP Conf. Ser. Mater. Sci. Eng. 114, 012109.

du Plessis, A., le Roux, S.G., Steyn, F., 2016. Quality Investigation of 3D Printer Filament Using Laboratory X-Ray Tomography. 3D Print. Additive Manuf. 3, 262–267.

Futama, H., Tanaka, H., 1957. The Thermal Decomposition of Polyvinyl Alcohol Using Mass Spectrometer. J. Phys. Soc. Jpn. 12 433-433.

Goyanes, A., Buanz, A.B., Basit, A.W., Gaisford, S., 2014. Fused-filament 3D printing (3DP) for fabrication of tablets. Int. J. Pharm. 476, 88–92.

Goyanes, A., Buanz, A.B., Hatton, G.B., Gaisford, S., Basit, A.W., 2015a. 3D printing of modified-release aminosalicylate (4-ASA and 5-ASA) tablets. Eur. J. Pharm. Biopharm. 89, 157–162.

Goyanes, A., Martinez, P.R., Buanz, A., Basit, A.W., Gaisford, S., 2015b. Effect of geometry on drug release from 3D printed tablets. Int. J. Pharm. 494, 657–663.

Goyanes, A., Wang, J., Buanz, A., Martínez-Pacheco, R., Telford, R., Gaisford, S., Basit, A.W., 2015c. 3D printing of medicines: engineering novel oral devices with unique design and drug release characteristics. Mol. Pharm. 12, 4077–4084.

Kempin, W., Franz, C., Koster, L.-C., Schneider, F., Bogdahn, M., Weitschies, W., Seidlitz,

A., 2017. Assessment of different polymers and drug loads for fused deposition modeling of drug loaded implants. Eur. J. Pharm. Biopharm. 115, 84–93.
Khaled, S.A., Burley, J.C., Alexander, M.R., Roberts, C.J., 2014. Desktop 3D printing of controlled release pharmaceutical bilayer tablets. Int. J. Pharm. 461, 105–111.
Khaled, S.A., Burley, J.C., Alexander, M.R., Yang, J., Roberts, C.J., 2015a. 3D printing of five-in-one dose combination polypill with defined immediate and sustained release profiles. J. Control. Release 217, 308–314.
Khaled, S.A., Burley, J.C., Alexander, M.R., Yang, J., Roberts, C.J., 2015b. 3D printing of tablets containing multiple drugs with defined release profiles. Int. J. Pharm. 494, 643–650.
Markl, D., Zeitler, J.A., Rasch, C., Michaelsen, M.H., Müllertz, A., Rantanen, J., Rades, T., Bøtker, J., 2017. Analysis of 3D Prints by X-ray Computed Microtomography and Terahertz Pulsed Imaging. Pharm. Res. 34, 1037–1052.
Melocchi, A., Parietti, F., Loreti, G., Maroni, A., Gazzaniga, A., Zema, L., 2015. 3D printing by fused deposition modeling (FDM) of a swellable/erodible capsular device for oral pulsatile release of drugs. J. Drug Delivery Sci. Technol. 30, 360–367.
Mohsin, M., Hossin, A., Haik, Y., 2011. Thermomechanical properties of poly (vinyl alcohol) plasticized with varying ratios of sorbitol. Mater. Sci. Eng., A 528, 925–930.
Morita, R., Honda, R., Takahashi, Y., 2000. Development of oral controlled release preparations, a PVA swelling controlled release system (SCRS). II. In vitro and in vivo evaluation. J. Control. Release 68, 115–120.
Okwuosa, T.C., Pereira, B.C., Arafat, B., Cieszynska, M., Isreb, A., Alhnan, M.A., 2017. Fabricating a Shell-Core Delayed Release Tablet Using Dual FDM 3D Printing for Patient-Centred Therapy. Pharm. Res. 34, 427–437.
Okwuosa, T.C., Stefaniak, D., Arafat, B., Isreb, A., Wan, K.-W., Alhnan, M.A., 2016. A lower temperature FDM 3D printing for the manufacture of patient-specific immediate release tablets. Pharm. Res. 33, 2704–2712.
Sadia, M., Sośnicka, A., Arafat, B., Isreb, A., Ahmed, W., Kelarakis, A., Alhnan, M.A., 2016. Adaptation of pharmaceutical excipients to FDM 3D printing for the fabrication of patient-tailored immediate release tablets. Int. J. Pharm. 513, 659–668.
Skowyra, J., Pietrzak, K., Alhnan, M.A., 2015. Fabrication of extended-release patient-tailored prednisolone tablets via fused deposition modelling (FDM) 3D printing. Eur. J. Pharm. Sci. 68, 11–17.
Tagami, T., Fukushige, K., Ogawa, E., Hayashi, N., Ozeki, T., 2017. 3D Printing Factors Important for the Fabrication of Polyvinylalcohol Filament-Based Tablets. Biol. Pharm. Bull. 40, 357–364.